

SUPPLEMENTARY INFORMATION

S1. BOS04-5B core details

Extraction of the BOS04-5B sediment succession took place between July and October of 2004. Drill sites were chosen following a series of geophysical, seismic, and limnological studies conducted between 2000-2002, and drilling operations divided into two main parts: sediment (first two months), and the hard-rock (impactite and bedrock) (Karp et al., 2002; Koeberl et al., 2007b, 2005). Drilling was performed using the DOSECC/ICDP GLAD800 system custom-built specifically for lake drilling, from which twenty-three sediment cores, and two hard-rock (impactite) cores were obtained in the course of the 2004 ICDP drilling project (full details in Koeberl et al., (2005). This study focuses on the upper ~47 m section of a 296-m-long core extracted from deep-water (76 m) site 5 (core BOS04-5B). The core extends from the present-day lake floor to the brecciated bedrock, includes a basal sediment layer of impact-glass bearing accretionary lapilli with a thickness of ~30 cm, and has been dated by $^{40}\text{Ar}/^{39}\text{Ar}$ to 1.08 ± 0.04 Ma (Jourdan et al., 2009).

After drilling, the cores were shipped to the University of Rhode Island, where they were split, described, imaged, and analysed using a Geotek® multi-sensor core logger for a suite of magnetic and physical parameters. The cores were sampled for analysis of sediment magnetic hysteresis, x-ray diffraction mineralogy, total organic and inorganic carbon content, bulk organic carbon and nitrogen isotopes, and grain size. Core logging and physical sediment properties were used to develop a standardized depth scale for core 5B: permitting comparison between holes (e.g., site 5b and 5c) and coring locations (e.g., site 4, site 5) (Shanahan et al., 2013). Core depths presented in this paper are in meters below lake floor.

S2. Chronology

The BOSMORE7 model (Gosling et al., 2022) provides a newer, updated age-depth relationship for the BOS04-5B core compared to those earlier presented by Shanahan et al. (2013) and Miller et al. (2016). First, because it integrates the $^{39}\text{Ar}/^{40}\text{Ar}$ -derived crater age of 1.07 ± 0.11 Ma (Jourdan et al., 2009; Koeberl et al., 1997) to generate more robust age uncertainties for the deeper core sections. Second, because it does not include the six paleomagnetic excursions (Mono Lake, Laschamp, 4-a, 5-a, 5-b, 6-a) previously used as tie-points, owing to uncertainties in the reliability of these dates (Gosling et al., 2022). An age-depth relationship was constructed using a Bayesian approach in R, from which the model provided an ensemble of possible age models, their analytical age uncertainties, and sedimentation rates (Blaauw and Christen, 2011). The code used in model generation is available from: <https://doi.org/10.6084/m9.figshare.18319466>).

In 2024, Vinnepand and colleagues used cyclicity in total natural gamma ray (NGR) data to create a cyclostratigraphic age-depth model for the full (~946-kyr) BOS04-5B core. This model will be key for study of the deeper (>200 ka) core sections where fewer absolute age markers are available

(Shanahan et al. 2013). However, it is significantly lower resolution than the BOSMORE7 chronology in the upper ~47 m of the record, given that Vinnepand et al. (2024) did not include ^{14}C ages in their model generation. Not only does this limit the extent to which it can account for the high variability in Lake Bosumtwi's sedimentation regime during the Late Pleistocene (e.g., Shanahan et al. 2013; McKay, 2012), but it also creates a >10-kyr offset from the BOSMORE7 chronology for sediments >30 m depth. An offset that, in combination with ~10-kyr uncertainties for each of the three tie points in the upper 50 m of the core, substantially reduces the overall precision of the model with respect to our study interval. It does create substantial discrepancies. Therefore, given that the BOSMORE7 model explicitly includes absolute dating points and their uncertainties within the here studied interval, it provides age control for our data that is entirely independent from assumptions about past environmental conditions, and unaffected by any age uncertainty stemming from inter-site correlations.

S3: Mercury measurements

Total Hg (Hg_T) in the bulk sediments of core BOS04-5B was measured using the RA-915 Portable Mercury Analyzer with PYRO-915+ Pyrolyzer, Lumex (Bin et al., 2001) at the University of Oxford. This instrument required that the lacustrine sediment samples were dried prior to analysis, for which prior studies have used a range of techniques. These have included freeze-drying (Daga et al., 2016; Guéron et al., 2019; Hermanns and Biester, 2013; Ribeiro Guevara et al., 2010), high-temperature (Pérez-Rodríguez et al., 2019), and low-temperature oven drying (de Lacerda et al., 2017; Gelety et al., 2007). To determine if/how heat exposure may affect sedimentary concentrations of Hg in soft recent lacustrine sediments such as those from BOS04-5B, a pilot study was conducted using externally sourced, homogenous material. Approximately 14cm^3 of soft, muddy material was separated and subjected to different drying conditions. Samples (in triplicate) were dried at three temperatures, respectively: groups E1 and E3 at 40°C (oven), group E2 at 100°C (oven), and group C1 at -50°C (freeze dryer). Exposure times were also systematically varied between samples, ranging from one day (E2), to 1 week (E1 and C1), and four weeks (E3). Once dry, samples were ground using a mortar and pestle to produce a homogenous powder, and six Hg analyses (method described in section 3.4) were conducted for each group with three vials run as duplicates.

Our results showed a weak correlation between exposure temperature and Hg concentration ($r^2 = 0.09$). The lowest mean Hg concentrations were measured in the samples dried at 100°C , which could allude to Hg release during heating. Nonetheless, the results suggest that drying temperature does not strongly affect sedimentary Hg concentrations, with mean values across all four groups ranging from 27–30 ng g^{-1} . Following these results, BOS04-5B samples were prepared by oven-drying at 30°C for 72 hours before grinding the sediment to powder form, as this presented the quickest, least resource-intensive option and posed no risk of Hg loss.

S4: TOC measurements

To measure TOC contents of the BOS04-5B succession, powdered sediment samples were split into two aliquots and weighed. Weights for aliquot 1 were between 50-70 mg, and aliquot 2 between 90-120 mg. Prior to coulometric analysis, samples in aliquot 2 were furnace for 24 hours at 420°C in order to remove organic carbon fractions. Both aliquots were then combusted in oxygen at 1220 °C to break down the calcium carbonate and produce carbon dioxide (CO₂), which was fed into a solution of barium perchlorate. This would result in a change in the solution pH from an initial value of 10.0, following which back titration to the original pH using electrolysis gives a measure of the amount of carbon originally present – quantified by the amount of electricity required to restore a pH of 10.0, and recorded in counts (Jenkyns, 1988; Jenkyns and Weedon, 2013). Counts obtained for Aliquots 1 and 2 were used to calculate the total carbon (TC) content of the sample in wt.%, using the formula:

$$TC = \frac{\text{total counts} \times 0.2}{M} \quad (S1)$$

...whereby M is the sample mass in mg.

TOC were calculated as:

$$TOC = TC_1 - TC_2 \quad (S2)$$

... whereby TC₁ and TC₂ represent the TC values obtained for aliquots (1) and (2), respectively.

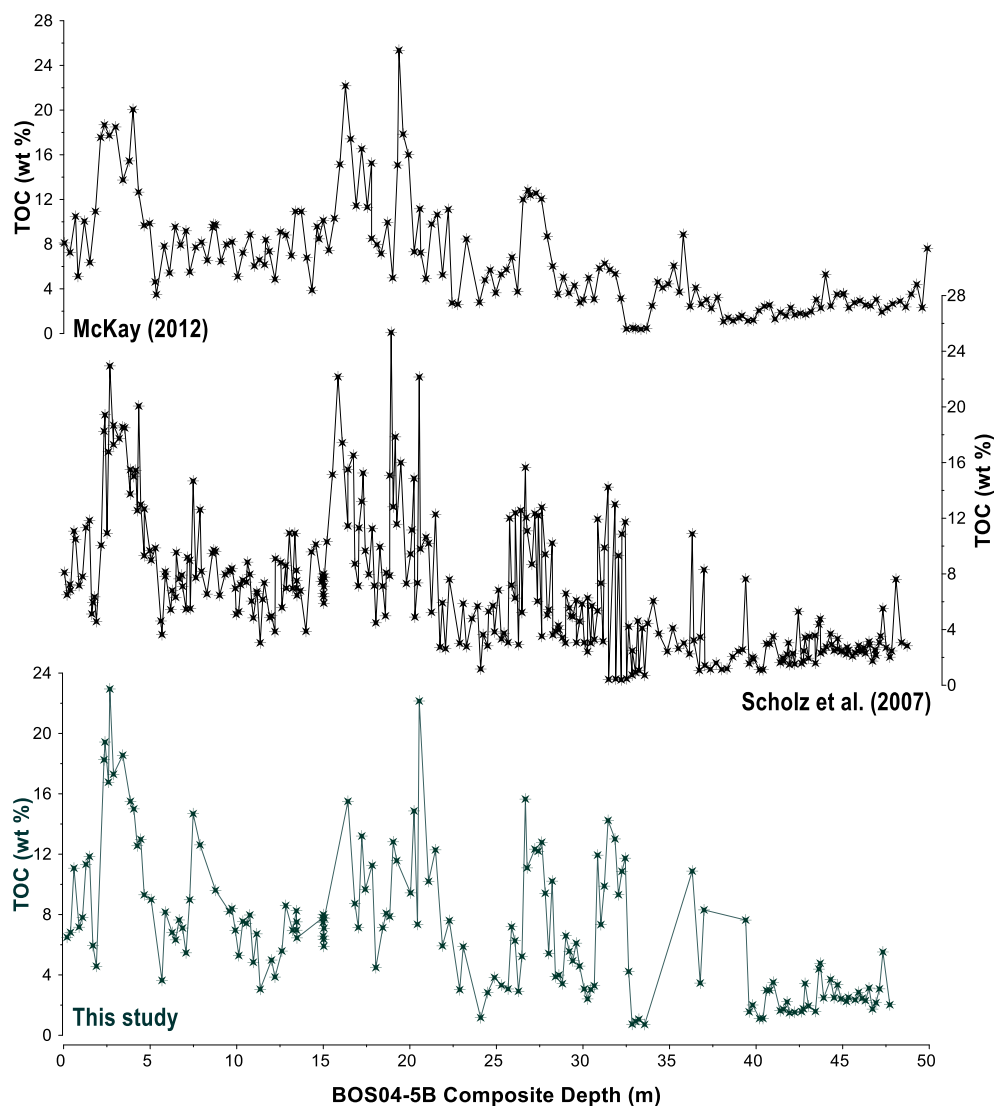


Figure S1: A comparison of TOC datasets for the upper 47 m of core BOS04-5B, obtained by loss-on-ignition (McKay, 2012; Scholz et al., 2007), and coulometry (*this study*). Sampling points are marked by stars on all three plots.

91 S5: Authigenic carbonates

92 The BOS04-5B core contains (mangano-) siderite in variable amounts (McKay, 2012; Shanahan et al.
 93 2008). These siderite-bearing intervals can be easily identified using bulk chemistry (e.g., XRF data),
 94 as Mn is unlikely to be a significant component of other sedimentary minerals (**Fig. S2**). Siderites
 95 commonly form in freshwater settings at shallow sediment depths under anaerobic (anoxic) conditions
 96 accompanied by organic-rich sediments (Armenteros, 2010; Sebag et al., 2018). However, these
 97 materials can make accurate measurement of organic carbon content in lacustrine sediment via
 98 pyrolysis- or furnace-based methods more challenging, as thermal decomposition of siderite typically
 99 starts at temperatures <420°C (Sebag et al., 2018): lower than that which is used to remove the
 100 organic fraction on the Coulomat (Jenkyns, 1988). This means that any siderite-sourced carbon
 101 released would lead to systematic overestimation of total organic carbon (Sebag et al., 2018).

Preliminary (repeat) analyses of a Jurassic-age siderite nodule (~ 85% siderite by weight, n=4) showed near-complete (>95%) siderite decomposition (carbonate-carbon loss) after furnacing overnight at 420 °C. We then removed siderites from sixteen BOS04-5B samples spanning a range of low-high Mn counts using a weak acid (warm 5% HCl) treatment, following the established methodologies of Brodie et al. (2011) and Vinduřková et al. (2019), and compared acid-treated and furnaced samples to assess the impact on TOC measurements for Bosumtwi material. The difference between untreated and treated samples ranged between -1.6 % and 1.38 %, which aligns with the expected difference between acid-treatment and pyrolysis-based methods for very organic-rich sediments. There was, however, no systematic offset nor a clear correlation with the Mn counts from XRF data (**Fig. S2c**), suggesting that the carbon release from siderite did not appreciably bias TOC measurements in our record.

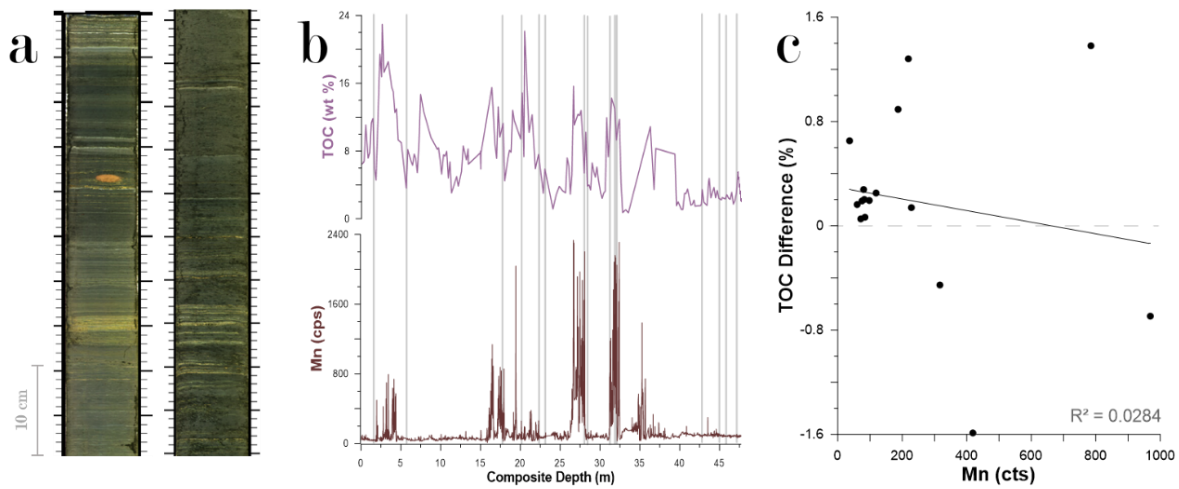


Figure S2: (a) Scan images of select sections of core BOS04-5B from Lake Bosumtwi, showing clear yellow-white carbonate layers. (b) Comparison of Mn abundance (McKay, 2012) and total organic carbon (TOC) (*this study*) data. (c) Relationship between Mn abundance, and the difference between TOC_U and TOC_T.

S6: Correlation analyses

Pearson correlation coefficients (r) were calculated for the BOS04-5B XRF dataset from the following equation:

$$r = \frac{\sum_{i=1}^n (x_i - \bar{x})(y_i - \bar{y})}{\sqrt{\sum_{i=1}^n (x_i - \bar{x})^2} \sqrt{\sum_{i=1}^n (y_i - \bar{y})^2}} \quad (S3)$$

...where x_i and y_i are the individual data points for the two variables, \bar{x} and \bar{y} are the means of the x and y datasets, and n is the number of data points (157).

The resulting coefficient values indicate the direction and strength of the association between a two-element pair, where $r = -1$ represents a perfect negative association, $r = 0$ represents no association,

and $r = 1$ represents a perfect positive association. Thus, higher values suggest that similar processes influenced the concentration of the two elements in tandem.

The significance of the correlations presented in **Figure 3b** were assessed using a Student's t statistical test, where Pearson's coefficient values (r) were first converted to a t -statistic using:

$$t = \frac{r \times \sqrt{n-2}}{\sqrt{1-r^2}} \quad (S4)$$

...where r is the correlation coefficient value, and n is the number of pairs in the test (157 for BOS04-5b). These t -statistic values were converted to p -values using the TDIST function in Microsoft Excel:

$$p = TDIST(x, DF, tails) \quad (S5)$$

...where x values represent the t -values obtained using eqn. 1, ***tails*** signify the two-tailed probability test (here taken as 2), and ***DF*** stands for degrees of freedom, which is calculated as:

$$DF = n - 2 \quad (S6)$$

S7. Change point analyses

To test the significance of the shifts in Hg_T identified, and discussed in our manuscript, we used Paleontological Statistics Software (PAST) v.4.16 to apply a change point analysis function to the BOS04-5B data (Hammer et al. 2001). The PAST software uses a Bayesian Markov chain Monte Carlo (MCMC) approach, which estimates parameters by sampling from their probability distributions rather than providing a single fixed result. By producing a large number of samples from the probability distribution, the algorithm provides not just the most probable model based on the given data, but also insights into the uncertainty and variability in the results. For example, a step-like curve will be produced if the majority of simulations agree on the changepoint positions, and greater uncertainty in changepoint positions will produce a more rounded appearance. Given the large range in Hg_T values exhibited by our data, a total of 1 million MCMC simulations were run, with a ≤ 10 changepoint limit.

This analysis highlights two distinct shifts in the Hg_T data. The first between ~ 75 and 72 ka, and the second between 12.6 and 3.7 ka (**Fig. S3**). These two shifts remained significant and visible even when the maximum changepoint value was lowered; only when this number became < 3 did the change between ~ 75 and 73 ka become invisible, following which the sapropel-correlated signal became dominant. These signals each correspond to Arid Interval-1 (AI-1) and sapropel layer 1, respectively, and so confirm the significance of the visual changes in the Hg_T curve during these two intervals.

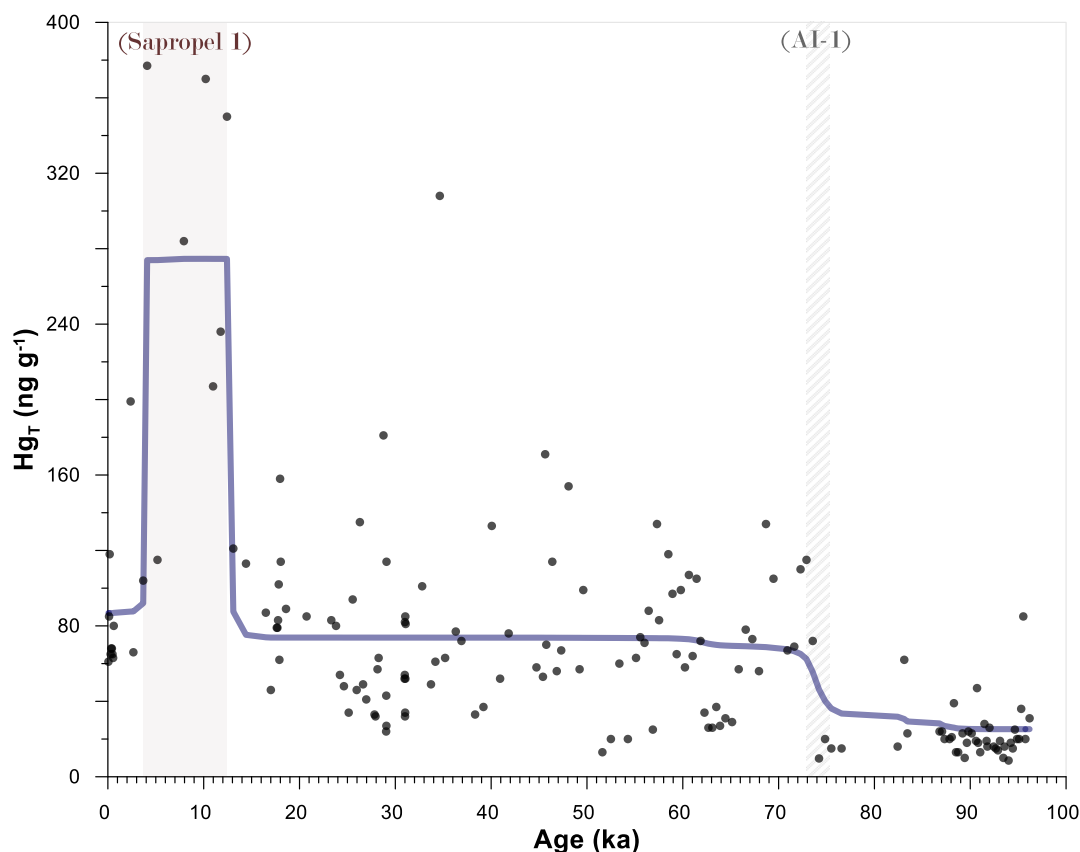


Figure S3: The average changepoint model for BOS04-5B displayed as a purple curve, superimposed onto the original Hg_T values. The abruptness of the curve indicates the extent to which the MCMC simulations ($n = 1000000$) agree on the changepoint positions, where greater smoothing indicates greater variance between simulations. Unit AI-1 is marked between 33.5 and 32.8 m depth (grey shading; Brooks et al., 2005; Scholz et al., 2007), and sapropel layer 1 is marked between 3–5.5 m depth (brown shading; Shanahan et al., 2012, 2006).

S8: Variations in Hg host phases with time

Time-resolved variability in the degree of covariation between Hg, TOC, and detrital matter was explored by means of a simple rolling-window (RW) correlation analysis, which has been highlighted as an effective tool for exploration of compositional variability through time (Oehlert and Swart, 2019; Sun et al., 2021; Ulfers et al., 2022; Wang et al., 2014). Applying this technique to the BOS04-5B Hg data permits a broad assessment of variability in Hg host-phase relationships in this system through time, identify any measurable changes that could reflect major changes in Hg burial dynamics, and elucidate the potential mechanisms responsible for these changes. Once Pearson correlation coefficients between the Hg, TOC, and K_{clr} data had calculated, time series profiles were then averaged across two window sizes - ~1-kyr and ~10-kyr (**Fig. S4**).

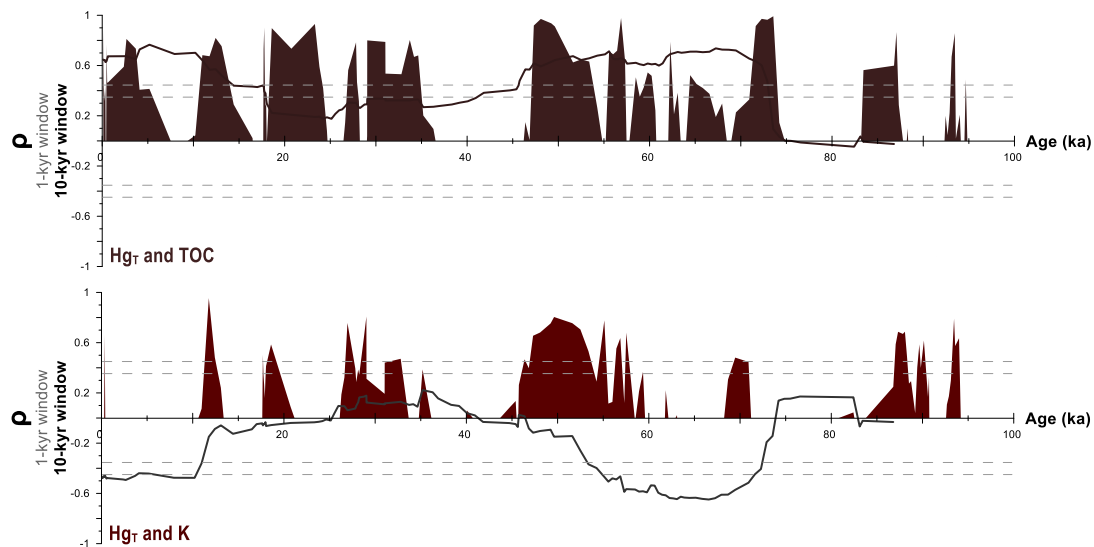


Figure S4: Pearson's correlation coefficients (ρ) between total Hg (Hg_T) and centered-log ratio corrected potassium (K_{clr}), and Hg_T and organic matter (TOC) data from core BOS04-5B from Lake Bosumtwi. Significance bands are marked with dashed grey lines ($\pm 20\%$), and shaded areas indicate periods of high correlation where R values exceed the upper limit of this threshold. A ~ 1 -kyr window size corresponds to a stratigraphic resolution of ~ 1 m, and a ~ 10 -kyr window size to a stratigraphic resolution of ~ 10 m.

The Hg and TOC relationship identified by linear correlation analysis (**Fig. S4**) appears consistently positive throughout the succession. Focussing on the ~ 10 -kyr series, R values typically range between ~ 0.9 and 0.2 with only transient instances where this value drops < 0.2 . Conversely, the Hg/K_{clr} profile shows a consistently negative relationship between Hg_T and the detrital fraction in BOS04-5B (**Fig. S4**), which fluctuates in an antithetical manner to the Hg and TOC profile. For example, the weakest correlation between Hg and the detrital fraction is observed when the Hg and TOC relationship is strongest between ~ 73 and 45 ka (**Fig. S4**). Nonetheless, a common feature between the two plots is a broad downward trend in the correlation coefficients through time, with the highest values generally observed in the deeper (older) core sections (**Fig. SF4**). Variability through time is significantly more pronounced for the ~ 1 -kyr-window profiles. Sporadic, high-amplitude peaks at discrete points throughout the record show transient instances whereby the correlation between Hg, organic matter and/or detrital influx changes measurably, suggesting that Hg signals recorded in Lake Bosumtwi since ~ 100 ka could also reflect changes in the net flux of Hg into the system, and not solely host phase availability.

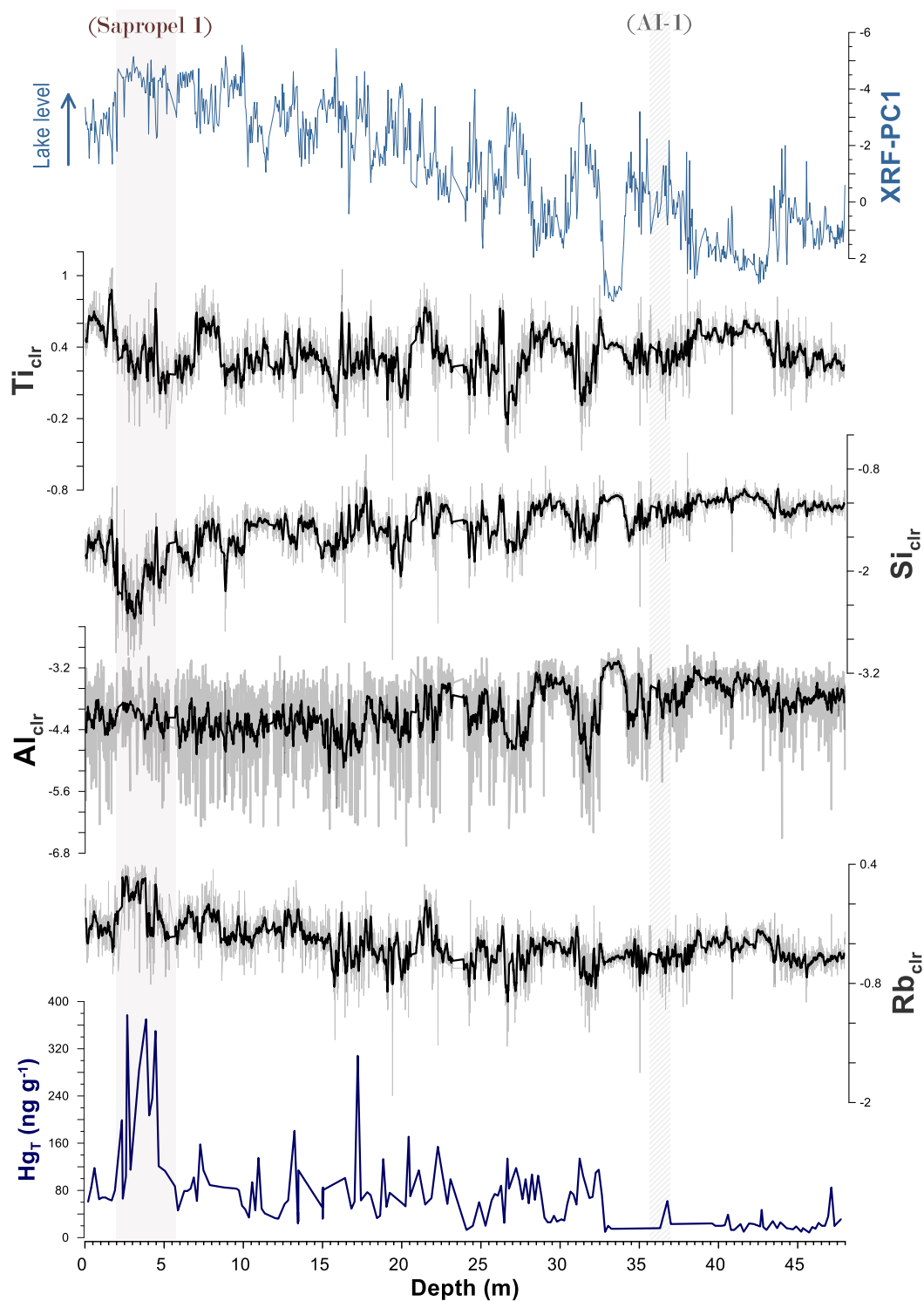


Figure S5: A record of Hg_T (this study) for the upper ~47 m of core BOS04-5B, compared with X-ray fluorescence data measured using XRF by McKay (2012), and corrected using a centered-log ratio (clr) approach (Bertrand et al. 2024): all signaling changes detrital material influx into the basin.

S9: Proxy records

Table S1: Details of proxy records displayed in **Figure 5** (main text).

Core	Location	Latitude	Proxy	Interpretation	Reference(s)
GeoB7920	Atlantic Ocean	20°N	Humidity Index (HI)	Grain-size distribution of the siliciclastic sediment fractions were used to derive proportions of three statistically relevant endmembers: coarse aeolian dust (EM1), fine aeolian dust (EM2), and hemi-pelagic mud (EM3). EM3 can be related to fluvial transport, and the proportions of aeolian endmembers EM1 and EM2 to subaerial erosion and vegetation cover. Authors use the log ratios of EM3, EM1 and EM2 ($\log[EM3/(EM1 + EM2)]$) to derive an index reflecting relative changes of the continental humidity and vegetation cover.	(Tjallingii et al., 2008)
ODP 927	Mediterranean Sea	34°N	Ti/Al	Ti/Al in the open Eastern Mediterranean reflects relative variations in North African aeolian vs riverine inputs to the basin. Aeolian-sourced Ti/Al in the open Eastern Mediterranean is enhanced relative to fluvially-sourced Ti/Al because heavier (Ti-bearing) suspended particles preferentially settle near the Nile fan. Al normalisation (for Ti and Ba) also removes closed-sum effects. Higher values signal an aeolian source, lower values signal a fluvial source.	(Grant et al., 2022, 2017)
ODP658	Atlantic Ocean	20°N	Dust fluxes	Reflects aeolian (mineral) dust export from the Sahara desert, and broader variations in wind strength, wind speed, African monsoon intensity, humidity, and atmospheric circulation dynamics.	(Kinsley et al., 2022)
MD03-2705	Atlantic Ocean	18°N	Dust fluxes	Reflects aeolian (mineral) dust export from the Sahara desert, and broader variations in wind strength, wind speed, African monsoon intensity, humidity, and atmospheric circulation dynamics.	(Skonieczny et al., 2019)
MD03-2621	Cariaco Basin	10°N	Reflectance (L^*)	Sediment reflectance as a proxy for terrigenous sediment deposition into the ocean. Light/dark coloured laminations capture seasonally varying sediment inputs into the basin, modulated by ITCZ dynamics.	(Deplazes et al., 2013)
MD03-2707	Gulf of Guinea	2°N	Sea-surface temperature	Large-scale changes in West African monsoon precipitation and riverine runoff are reflected in the isotopic and barium (Ba) composition of seawater and budget of dissolved Ba in Gulf of Guinea which is, in turn, archived in microfossils that accumulate in marine sediments.	(Weldeab et al., 2007)

S10: Crater origin and geology

The Bosumtwi crater was formed by an asteroid impact 1.08 ± 0.04 Ma ago (**Fig. S6**; Jourdan et al., 2009; Koeberl et al., 1997). Evidence for low shock metamorphism and impact melt fragment abundance in Bosumtwi crater-sourced samples suggests the majority of heavily shocked material was ejected from the crater (Coney et al., 2007; Koeberl et al., 2007a), with evidence for distal material ejection ~300 km away (Koeberl et al., 2007a, 1997). On one hand, this vertical displacement of material may have caused the simultaneous vaporization and emission of geogenic Hg at the surface immediately following impact (Artemieva et al., 2017; Feignon et al., 2022). Quantitative estimates suggest that ~94,000–480,000 Mg Hg was emitted at the Earth's surface following the Chicxulub impact event (Artemieva et al., 2017; Fendley et al., 2019), and lithostratigraphic evidence for toasting of shocked quartz in the Bosumtwi crater suggest that the target rocks were particularly volatile-rich (Coney et al., 2007; Koeberl et al., 2007b). However, the extent to which the geogenic Hg pool may contribute to signals recorded in Lake Bosumtwi is difficult to constrain, given that impact breccias extracted from the basin show no measurable evidence for a meteoritic component in the Bosumtwi crater (Koeberl et al., 2007b); meaning that the Hg concentration of the Bosumtwi impactor remains unknown.

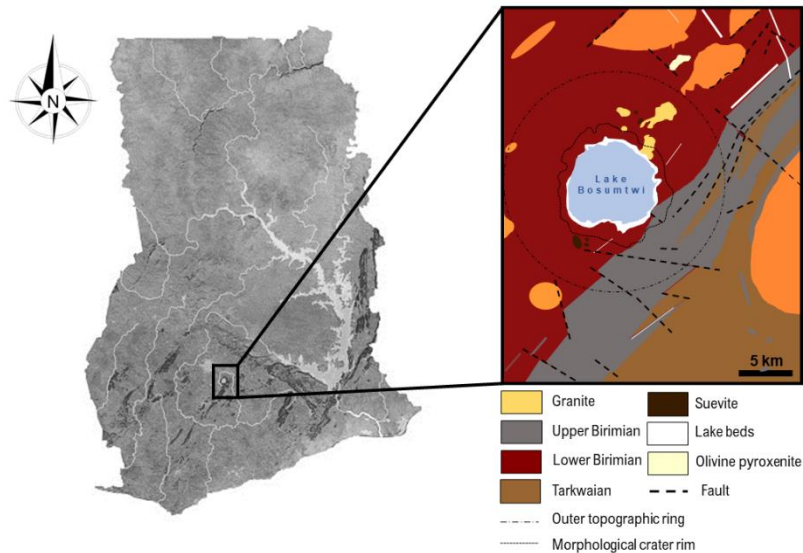


Figure S6: A schematic geological map of the Bosumtwi impact structure, Ghana. Adapted from Koeberl et al. (2007)

S11: Regional volcanism

Volcanic activity is a key component of the global Hg cycle (Pyle and Mather, 2003), and higher natural Hg concentrations in soil, air and bedrock found predominantly at or surrounding plate boundaries where tectonic, volcanic, and geothermal activities are most intense (Edwards et al., 2021; Rytuba, 2003; Schlüter, 2000). There are no active volcanoes in Ghana, however, Lake Bosumtwi is located in close proximity to several highly productive volcanic regions. These include the East African Rift Zone (Biggs et al., 2021; Pyle, 1999; Vidal et al., 2022), the Cameroon Volcanic Line (CVL), the Canary Islands, and Cape Verde (Pyle, 1999). Identification of cryptotephra produced by the ~74 ka eruption of Toba volcano (Indonesia) in Lake Malawi also highlights the potential for deposition of volcanogenic material over Africa originating from distal, exceptionally large eruptions (Lane et al., 2013). However, the resolution of BOS04-5B precludes our ability to examine Hg emissions with respect to single eruption events (**Fig. S7**). Although we do find a coincidence between the frequency of tropical volcanism and intervals of elevated Hg concentration in Lake Bosumtwi (**Fig. S7**), it is likely that this is a function of the progressive improvement in eruption recording with time (Colby et al., 2022; Fontijn et al., 2018; Vidal et al., 2022), and/or a global rise in Hg emissions resulting from industrial practices during the Holocene (United Nations Environment Programme, 2018): both of which could further increase wet deposition of Hg in the terrestrial realm. Taken together, eruption record incompleteness coupled with time-transgressive changes in the global atmospheric Hg burden both complicate the ability to unambiguously correlate enhanced volcanic emissions to greater Hg deposition in our record.

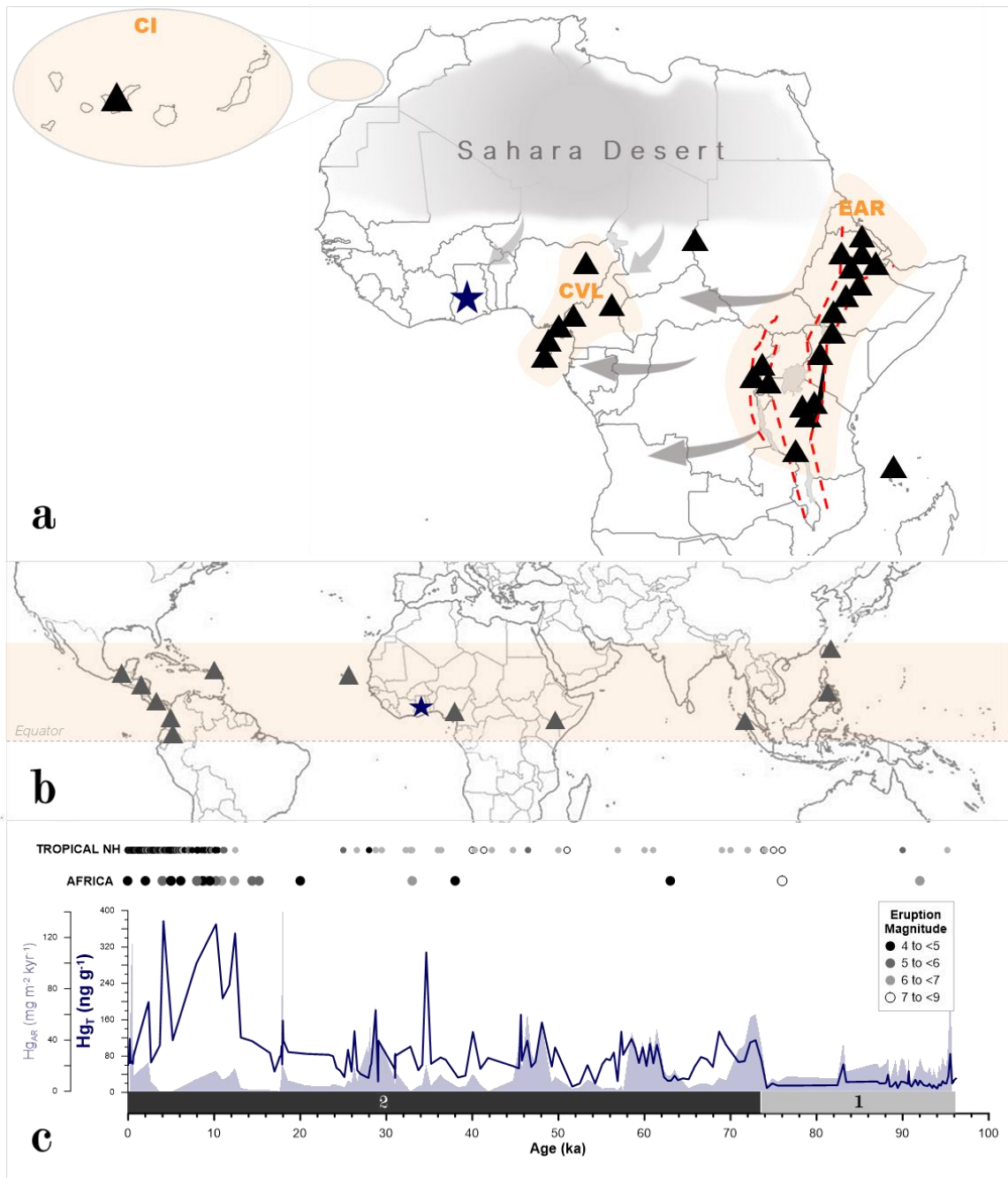


Figure S7: (a) Map of Africa showing volcanic regions with evidence for activity during the late Quaternary (< 100 ka): CI – Canary Islands, CVL – Cameroon Volcanic Line, EAR – East African Rift. Individual systems are marked as grey triangles, and the direction of major atmospheric circulation systems as grey arrows. Lake Bosumtwi is marked as a navy-blue star; (b) Map of the Northern Hemisphere. Black triangles mark volcanic regions possessing known eruptions (>magnitude 4.0) dated between 100–0 ka, as listed in the LaMEVE database (Croswell et al., 2012). Lake Bosumtwi is marked as a navy-blue star; (c) Time-resolved Hg accumulation rate (Hg_{AR}) and residual Hg (Hg_R) data for BOS04-5B (Lake Bosumtwi) compared to the number and timing of radiometrically-dated eruptions in Africa and the Northern Hemisphere, based on the LaMEVE database and regional tephrostratigraphic records. Circles denoting individual eruptions are coloured with respect to magnitude.

S12: Fire activity

Combustion of terrestrial vegetation is one way catchment-stored Hg may be re-emitted into the atmosphere (Bishop et al., 2020). Elemental Hg (Hg^0) retains a low re-volatilisation temperature of 100-300°C (Friedli et al., 2009), and the total amount of Hg released during a wildfire event will vary depending on the plant species' sink capacity (e.g., Kumar et al., 2018; Zhou et al., 2021). Thus, quantifying the severity, intensity (temperature), and primary fuel source of past fire activity has been posited to provide important information regarding wildfire contributions to changes in the terrestrial Hg cycle (Daga et al., 2016; Guédron et al., 2019). However, in Lake Bosumtwi, preliminary macrocharcoal analysis suggests that Hg sequestration is not directly coupled to wildfire intensity and/or frequency (**Fig. S8**) (Kiely, 2023). For example, high macrocharcoal particle counts coincide with some of the largest Hg peaks at ~36 ka, whereas fire appears completely absent between 3 and 0 ka: an interval in which the highest Hg concentrations are observed (**Fig. S8**). Moreover, peaks in concentration also often 'lag' behind macrocharcoal enrichments by ~2-kyr (**Fig. S8**), and so whether these two signals are mechanistically linked remains unclear.

There are several possible reasons for the observed lack of coherence between fire severity, intensity and Hg concentration in Lake Bosumtwi: (1) large quantities of particulate-bound Hg were emitted into the atmosphere during arid intervals, but were only deposited into the lake when precipitation was sufficiently heavy. Thus, following dissemination of the primary signal (Francisco López et al., 2022; Kumar et al., 2018; Melendez-Perez et al., 2014); (2) the lake's closed structure limited downstream transport of Hg released from burned soils and bound to fine and coarse particulate matter (Bishop et al., 2020; Jensen et al., 2017; Ku et al., 2018); and/or (3) fire-derived Hg signals were overprinted by more dominant processes influencing the sediment record (e.g., primary productivity, detrital mineral supply) (de Lacerda et al., 2017; Paine et al., 2024; Schütze et al., 2018). Although we cannot rule out the possibility that wildfire activity did affect Hg fluxes into the Lake Bosumtwi system, preliminary data suggest that other drivers were likely more influential; namely moisture-driven changes in sedimentation, productivity, and detrital material supply.

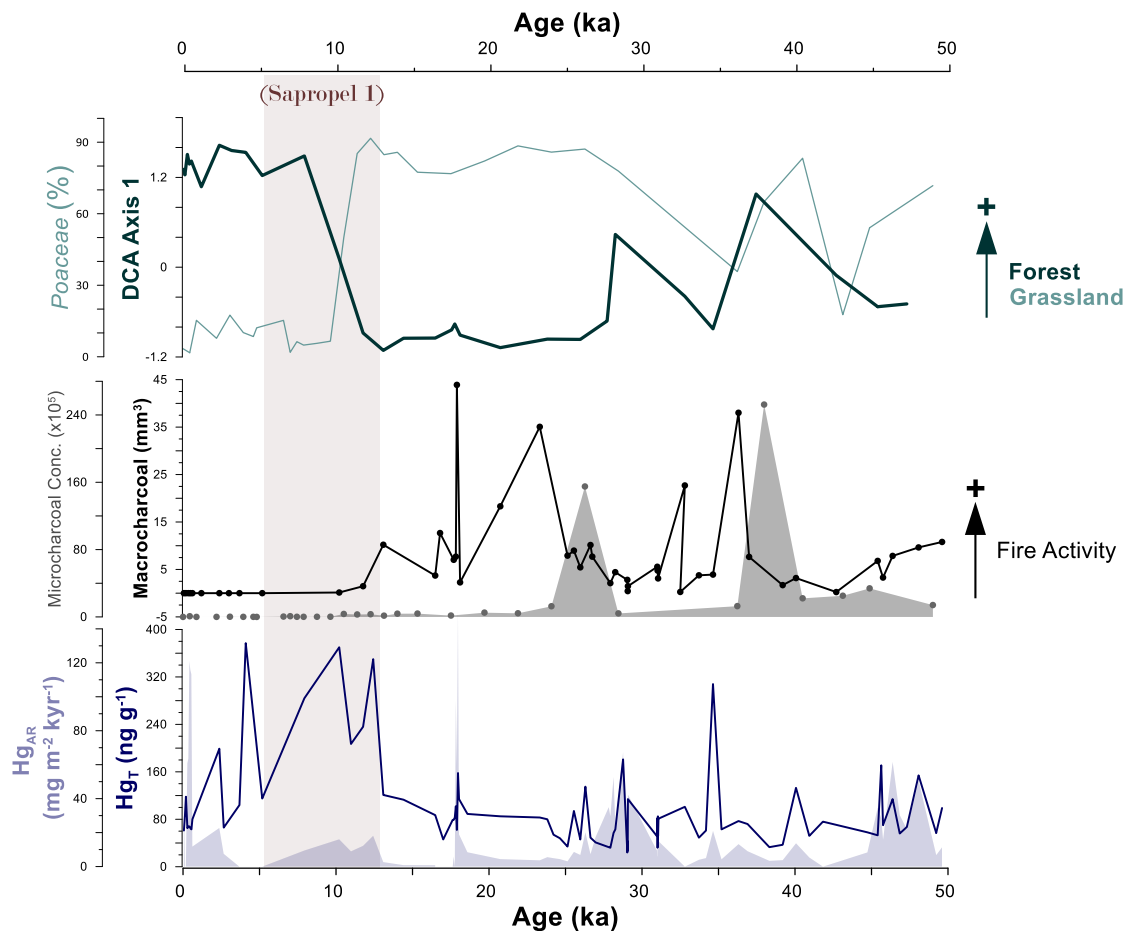


Figure S8: 50-kyr records of total mercury (Hg_T) and mercury accumulation rate (Hg_{AR}) for Lake Bosumtwi from this study, with proxy datasets from prior studies of the same lake. These include forest (woody) taxa abundance represented by detrended correspondence analysis (DCA) axis 1 (Gosling et al., 2022; Miller et al., 2016), percentage abundance of Poaceae (grass) pollen (Miller et al., 2016), microcharcoal concentrations (Miller et al., 2016), and macrocharcoal volume (Kiely, 2023). A distinct lake low stand (LS) based on seismic profiles and sedimentological data is marked between 33.5 and 32.8 m depth (grey shading) (Brooks et al., 2005; Scholz et al., 2007), and sapropel layer 1 is marked between 3–5.5 m depth (brown shading) (Shanahan et al., 2012, 2006). Unit Al-1 is marked between 33.5 and 32.8 m depth (grey shading) (Brooks et al., 2005; Scholz et al., 2007), and sapropel layer 1 is marked between 3–5.5 m depth (brown shading) (Shanahan et al., 2012, 2006).

241 References Cited

- 242 Armenteros, I.: Diagenesis of Carbonates in Continental Settings, in: Developments in Sedimentology. Elsevier,
 243 pp. 61–151. [https://doi.org/10.1016/S0070-4571\(09\)06202-5](https://doi.org/10.1016/S0070-4571(09)06202-5), 2010.
- 244 Artemieva, N., Morgan, J., and Expedition Party 364.: Quantifying the Release of Climate-Active Gases by Large
 245 Meteorite Impacts With a Case Study of Chicxulub. *Geophysical Research Letters* 44, 10180–10188.
 246 <https://doi.org/10.1002/2017GL074879>, 2017.
- 247 Bahr, D.B., Hutton, E.W.H., Syvitski, J.P.M., and Pratson, L.F.: Exponential approximations to compacted
 248 sediment porosity profiles. *Computers & Geosciences* 27, 691–700. [https://doi.org/10.1016/S0098-3004\(00\)00140-0](https://doi.org/10.1016/S0098-3004(00)00140-0), 2001.
- 250 Bertrand, S., Tjallingii, R., Kylander, M.E., Wilhelm, B., Roberts, S.J., Arnaud, F., Brown, E., and Bindler, R.:
 251 Inorganic geochemistry of lake sediments: A review of analytical techniques and guidelines for data
 252 interpretation. *Earth-Science Reviews* 249, 104639. <https://doi.org/10.1016/j.earscirev.2023.104639>,
 253 2024.

- Biggs, J., Ayele, A., Fischer, T.P., Fontijn, K., Hutchison, W., Kazimoto, E., Whaler, K., and Wright, T.J.: Volcanic activity and hazard in the East African Rift Zone. *Nature Communications* 12, 1–12. <https://doi.org/10.1038/s41467-021-27166-y>, 2021.
- Bin, C., Xiaoru, W., and Lee, F.S.C.: Pyrolysis coupled with atomic absorption spectrometry for the determination of mercury in Chinese medicinal materials. *Analytica Chimica Acta* 447, 161–169. [https://doi.org/10.1016/S0003-2670\(01\)01218-1](https://doi.org/10.1016/S0003-2670(01)01218-1), 2001.
- Bishop, K., Shanley, J.B., Riscassi, A., de Wit, H.A., Eklöf, K., Meng, B., Mitchell, C., Osterwalder, S., Schuster, P.F., Webster, J., and Zhu, W.: Recent advances in understanding and measurement of mercury in the environment: Terrestrial Hg cycling. *Science of the Total Environment* 721. <https://doi.org/10.1016/j.scitotenv.2020.137647>, 2020.
- Blaauw, M., and Christen, J.A.: Flexible paleoclimate age-depth models using an autoregressive gamma process. *Bayesian Analysis* 6, 457–474. <https://doi.org/10.1214/11-BA618>, 2011.
- Bonk, A., Stowiński, M., Żarczyński, M., Oliński, P., Kupryjanowicz, M., Filoc, M., and Tylmann, W.: Tracking fire activity and post-fire limnological responses using the varved sedimentary sequence of Lake Jaczno, Poland. *The Holocene* 32, 515–528. <https://doi.org/10.1177/09596836221080755>, 2022.
- Brodie, C.R., Leng, M.J., Casford, J.S.L., Kendrick, C.P., Lloyd, J.M., Yongqiang, Z., and Bird, M.I.: Evidence for bias in C and N concentrations and $\delta^{13}\text{C}$ composition of terrestrial and aquatic organic materials due to pre-analysis acid preparation methods. *Chemical Geology* 282, 67–83. <https://doi.org/10.1016/j.chemgeo.2011.01.007>, 2011.
- Brooks, K., Scholz, C.A., King, J.W., Peck, J., Overpeck, J.T., Russell, J.M., and Amoako, P.Y.O.: Late-Quaternary lowstands of lake Bosumtwi, Ghana: Evidence from high-resolution seismic-reflection and sediment-core data. *Palaeogeography, Palaeoclimatology, Palaeoecology* 216, 235–249. <https://doi.org/10.1016/j.palaeo.2004.10.005>, 2005.
- Brown, S.K., Croswell, H.S., Sparks, R.S.J., Cottrell, E., Deligne, N.I., Guerrero, N.O., Hobbs, L., Kiyosugi, K., Loughlin, S.C., Siebert, L., and Takarada, S.: Characterisation of the Quaternary eruption record: Analysis of the Large Magnitude Explosive Volcanic Eruptions (LaMEVE) database. *Journal of Applied Volcanology* 3, 1–22. <https://doi.org/10.1186/2191-5040-3-5>, 2014.
- Clark, J.S., and Hussey, T.C.: Estimating the mass flux of charcoal from sedimentary records: effects of particle size, morphology, and orientation. *The Holocene* 6, 129–144. <https://doi.org/10.1177/095968369600600201>, 1996.
- Colby, D.J., Pyle, D.M., Fontijn, K., Mather, T.A., Melaku, A.A., Mengesha, M.A., and Yirgu, G.: Stratigraphy and eruptive history of Corbetti Caldera in the Main Ethiopian Rift. *Journal of Volcanology and Geothermal Research* 428, 107580. <https://doi.org/10.1016/j.jvolgeores.2022.107580>, 2022.
- Coney, L., Gibson, R.L., Reimold, W.U., and Koeberl, C.: Lithostratigraphic and petrographic analysis of ICDP drill core LB-07A, Bosumtwi impact structure, Ghana 589, 569–589, 2007.
- Croswell, H.S., Arora, B., Brown, S.K., Cottrell, E., Deligne, N.I., Guerrero, N.O., Hobbs, L., Kiyosugi, K., Loughlin, S.C., Lowndes, J., Nayembil, M., Siebert, L., Sparks, R.S.J., Takarada, S., and Venzke, E.: Global database on large magnitude explosive volcanic eruptions (LaMEVE). *Journal of Applied Volcanology* 1, 1–13. <https://doi.org/10.1186/2191-5040-1-4>, 2012.
- Daga, R., Ribeiro Guevara, S., Pavlin, M., Rizzo, A., Lojen, S., Vreča, P., Horvat, M., and Arribère, M.: Historical records of mercury in southern latitudes over 1600 years: Lake Futalaufquen, Northern Patagonia. *Science of the Total Environment* 553, 541–550. <https://doi.org/10.1016/j.scitotenv.2016.02.114>, 2016.
- de Lacerda, L.D., Turcq, B., Sifeddine, A., and Cordeiro, R.C.: Mercury accumulation rates in Caço Lake, NE Brazil during the past 20.000 years. *Journal of South American Earth Sciences* 77, 42–50. <https://doi.org/10.1016/j.jsames.2017.04.008>, 2017.
- Deplazes, G., Lückge, A., Peterson, L.C., Timmermann, A., Hamann, Y., Hughen, K.A., Röhl, U., Laj, C., Cane, M.A., Sigman, D.M., and Haug, G.H.: Links between tropical rainfall and North Atlantic climate during the last glacial period. *Nature Geoscience* 6, 213–217. <https://doi.org/10.1038/ngeo1712>, 2013.
- Edwards, B.A., Kushner, D.S., Outridge, P.M., and Wang, F.: Fifty years of volcanic mercury emission research: Knowledge gaps and future directions. *Science of the Total Environment* 757, 143800. <https://doi.org/10.1016/j.scitotenv.2020.143800>, 2021.
- Feignon, J.-G., Schulz, T., Ferriere, L., Goderis, S., Claeys, P., Graaff, S.J.D., Kaskes, P., De, T., and Koeberl, C.: Search for a meteoritic component within the impact melt rocks of the Chicxulub impact structure peak ring, Mexico. *Geochimica et Cosmochimica Acta* 323, 74–101. <https://doi.org/10.1016/j.gca.2022.02.006>, 2022.
- Fendley, I.M., Mittal, T., Sprain, C.J., Marvin-DiPasquale, M., Tobin, T.S., and Renne, P.R.: Constraints on the volume and rate of Deccan Traps flood basalt eruptions using a combination of high-resolution terrestrial mercury records and geochemical box models. *Earth and Planetary Science Letters* 524, 115721. <https://doi.org/10.1016/j.epsl.2019.115721>, 2019.
- Fitzgerald, W.F., Lamborg, C.H.: *Geochemistry of Mercury in the Environment*, Treatise on Geochemistry: Second Edition. Elsevier Ltd. <https://doi.org/10.1016/B978-0-08-095975-7.00904-9>, 2013.
- Fontijn, K., McNamara, K., Zafu Tadesse, A., Pyle, D.M., Dessalegn, F., Hutchison, W., Mather, T.A., and Yirgu, G.: Contrasting styles of post-caldera volcanism along the Main Ethiopian Rift: Implications for contemporary volcanic hazards. *Journal of Volcanology and Geothermal Research* 356, 90–113. <https://doi.org/10.1016/j.jvolgeores.2018.02.001>, 2018.
- Francisco López, A., Heckenauer Barrón, E.G., and Bello Bugallo, P.M.: Contribution to understanding the influence of fires on the mercury cycle: Systematic review, dynamic modelling and application to

- sustainable hypothetical scenarios. *Environ Monit Assess* 194, 707. <https://doi.org/10.1007/s10661-022-10208-3>, 2022.
- Friedli, H.R., Arellano, A.F., Cinnirella, S., and Pirrone, N.: Initial estimates of mercury emissions to the atmosphere from global biomass burning. *Environmental Science and Technology* 43, 3507–3513. <https://doi.org/10.1021/es802703g>, 2009.
- Gelety, V.F., Kalmykov, G.V., and Parkhomenko, I.Y.: Mercury in the sedimentary deposits of Lake Baikal. *Geochemistry International* 45, 170–177. <https://doi.org/10.1134/S001670290702005X>, 2007.
- Gosling, W.D., McMichael, C.N.H., Groenwood, Z., Roding, E., Miller, C.S., and Julier, A.C.M.: Preliminary evidence for green, brown and black worlds in tropical western Africa during the Middle and Late Pleistocene. *Palaeoecology of Africa* 35, 13–25. <https://doi.org/10.1201/9781003162766>, 2021.
- Gosling, W.D., Miller, C.S., Shanahan, T.M., Holden, P.B., Overpeck, J.T., and van Langevelde, Frank.: A stronger role for long-term moisture change than for CO₂ in determining tropical woody vegetation change. *Science* 376, 653–656. <https://doi.org/10.1126/science.abg4618>, 2022.
- Grant, K.M., Amarathunga, U., Amies, J.D., Hu, P., Qian, Y., Penny, T., Rodriguez-Sanz, L., Zhao, X., Heslop, D., Liebrand, D., Hennekam, R., Westerhold, T., Gilmore, S., Lourens, L.J., Roberts, A.P., and Rohling, E.J.: Organic carbon burial in Mediterranean sapropels intensified during Green Sahara Periods since 3.2 Myr ago. *Commun Earth Environ* 3, 11. <https://doi.org/10.1038/s43247-021-00339-9>, 2022.
- Grant, K.M., Grimm, R., Mikolajewicz, U., Marino, G., Ziegler, M., and Rohling, E.J.: The timing of Mediterranean sapropel deposition relative to insolation, sea-level and African monsoon changes. *Quaternary Science Reviews* 140, 125–141. <https://doi.org/10.1016/j.quascirev.2016.03.026>, 2016.
- Grant, K.M., Rohling, E.J., Westerhold, T., Zabel, M., Heslop, D., Konijnendijk, T., and Lourens, L.: A 3 million year index for North African humidity/aridity and the implication of potential pan-African Humid periods. *Quaternary Science Reviews* 171, 100–118. <https://doi.org/10.1016/j.quascirev.2017.07.005>, 2017.
- Guédron, S., Tolu, J., Brisset, E., Sabatier, P., Perrot, V., Bouchet, S., Develle, A.L., Bindler, R., Cossa, D., Fritz, S.C., and Baker, P.A.: Late Holocene volcanic and anthropogenic mercury deposition in the western Central Andes (Lake Chungará Chile). *Science of the Total Environment* 662, 903–914. <https://doi.org/10.1016/j.scitotenv.2019.01.294>, 2019.
- Hermanns, Y.M., and Biester, H.: A 17,300-year record of mercury accumulation in a pristine lake in southern Chile. *Journal of Paleolimnology* 49, 547–561. <https://doi.org/10.1007/s10933-012-9668-4>, 2013.
- Iverfeldt, A.: Mercury in forest canopy throughfall water and its relation to atmospheric deposition. *Water Air and Soil Pollution* 56, 553–564, 1991.
- Jenkyns, H.C.: The Early Toarcian (Jurassic) Anoxic Event. *American Journal of Science*, 1988.
- Jenkyns, H.C., and Weedon, G.P.: Chemostratigraphy (CaCO₃, TOC, $\delta^{13}\text{C}_{\text{org}}$) of Sinemurian (Lower Jurassic) black shales from the Wessex Basin, Dorset and palaeoenvironmental implications. nos 46, 1–21. <https://doi.org/10.1127/0078-0421/2013/0029>, 2013.
- Jensen, A.M., Scanlon, T.M., and Riscassi, A.L.: Emerging investigator series: The effect of wildfire on streamwater mercury and organic carbon in a forested watershed in the southeastern United States. *Environmental Science: Processes and Impacts* 19, 1505–1517. <https://doi.org/10.1039/c7em00419b>, 2017.
- Jourdan, F., Renne, P.R., and Reimold, W.U.: An appraisal of the ages of terrestrial impact structures. *Earth and Planetary Science Letters* 286, 1–13. <https://doi.org/10.1016/j.epsl.2009.07.009>, 2009.
- Karp, T., Milkereit, B., Janle, P., Danuor, S.K., Pohl, J., Berckhemer, H., and Scholz, C.A.: Seismic investigation of the Lake Bosumtwi impact crater: preliminary results. *Planetary and Space Science* 50, 735–743. [https://doi.org/10.1016/S0032-0633\(02\)00049-1](https://doi.org/10.1016/S0032-0633(02)00049-1), 2002.
- Kido, Y., Koshikawa, T., and Tada, R.: Rapid and quantitative major element analysis method for wet fine-grained sediments using an XRF microscanner. *Marine Geology* 229, 209–225. <https://doi.org/10.1016/j.margeo.2006.03.002>, 2006.
- Kiely, R.: A 50,000-year reconstruction of West African fire history (MSc Thesis). University of Amsterdam, Amsterdam, 2023.
- Kinsley, C.W., Bradtmiller, L.I., McGee, D., Galgay, M., Stuut, J.B., Tjallingii, R., Winckler, G., and DeMenocal, P.B.: Orbital and Millennial-Scale Variability in Northwest African Dust Emissions Over the Past 67,000 years. *Paleoceanography and Paleoclimatology* 37, 1–22. <https://doi.org/10.1029/2020PA004137>, 2022.
- Koeberl, C., Bottomley, R., Glass, B.P., and Storzer, D.: Geochemistry and age of Ivory Coast tektites and microtektites. *Geochimica et Cosmochimica Acta* 61, 1745–1772. [https://doi.org/10.1016/S0016-7037\(97\)00026-4](https://doi.org/10.1016/S0016-7037(97)00026-4), 1997.
- Koeberl, C., Brandstätter, F., Glass, B.P., Hecht, L., Mader, D., and Reimold, W.U.: Uppermost impact fallback layer in the Bosumtwi crater (Ghana): Mineralogy, geochemistry, and comparison with Ivory Coast tektites. *Meteoritics and Planetary Science* 42, 709–729. <https://doi.org/10.1111/j.1945-5100.2007.tb01069.x>, 2007a.
- Koeberl, C., Milkereit, B., Overpeck, J.T., Scholz, C.A., Amoako, P.Y.O., Boamah, D., Danuor, S.K., Karp, T., Kueck, J., Hecky, R.E., King, J.W., and Peck, J.A.: An international and multidisciplinary drilling project into a young complex impact structure: The 2004 ICDP Bosumtwi Crater Drilling Project - An overview. *Meteoritics and Planetary Science* 42, 483–511. <https://doi.org/10.1111/j.1945-5100.2007.tb01057.x>, 2007b.
- Koeberl, C., Peck, J., King, J., Milkereit, B., Overpeck, J., and Scholz, C.: The ICDP lake Bosumtwi drilling project: A first report. *Scientific Drilling* 1, 23–27. <https://doi.org/10.2204/iodp.sd.1.04.2005>, 2005.

- Ku, P., Tsui, M.T.-K., Nie, X., Chen, H., Hoang, T.C., Blum, J.D., Dahlgren, R.A., and Chow, A.T.: Origin, Reactivity, and Bioavailability of Mercury in Wildfire Ash. *Environ. Sci. Technol.* 52, 14149–14157. <https://doi.org/10.1021/acs.est.8b03729>, 2018.
- Kumar, A., Wu, S., Huang, Y., Liao, H., and Kaplan, J.O.: Mercury from wildfires: Global emission inventories and sensitivity to 2000–2050 global change. *Atmospheric Environment* 173, 6–15. <https://doi.org/10.1016/j.atmosenv.2017.10.061>, 2018.
- Lane, C.S., Chorn, B.T., and Johnson, T.C.: Ash from the Toba supereruption in Lake Malawi shows no volcanic winter in East Africa at 75 ka. *Proceedings of the National Academy of Sciences* 110. <https://doi.org/10.1073/pnas.1301474110>, 2013.
- McKay, N.P.: A multidisciplinary approach to late Quaternary paleoclimatology with an emphasis on sub-saharan West Africa and the last interglacial period (PhD Thesis). University of Arizona, Arizona, 2012.
- Melendez-Perez, J.J., Fostier, A.H., Carvalho, J.A., Windmüller, C.C., Santos, J.C., and Carpi, A.: Soil and biomass mercury emissions during a prescribed fire in the Amazonian rain forest. *Atmospheric Environment* 96, 415–422. <https://doi.org/10.1016/j.atmosenv.2014.06.032>, 2014.
- Miller, C.S., and Gosling, W.D.: Quaternary forest associations in lowland tropical West Africa. *Quaternary Science Reviews* 84, 7–25. <https://doi.org/10.1016/j.quascirev.2013.10.027>, 2014.
- Miller, C.S., Gosling, W.D., Kemp, D.B., Coe, A.L., and Gilmour, I.: Drivers of ecosystem and climate change in tropical West Africa over the past ~540 000 years. *Journal of Quaternary Science* 31, 671–677. <https://doi.org/10.1002/jqs.2893>, 2016.
- Moore, H.R., Crocker, A.J., Belcher, C.M., Meckler, A.N., Osborne, C.P., Beerling, D.J., and Wilson, P.A.: Hydroclimate variability was the main control on fire activity in northern Africa over the last 50,000 years. *Quaternary Science Reviews* 288, 107578. <https://doi.org/10.1016/j.quascirev.2022.107578>, 2022.
- Oehlert, A.M., and Swart, P.K.: Rolling window regression of $\delta^{13}\text{C}$ and $\delta^{18}\text{O}$ values in carbonate sediments: Implications for source and diagenesis. *Depositional Rec* 5, 613–630. <https://doi.org/10.1002/dep2.88>, 2019.
- Paine, A.R., Fendley, I.M., Frieling, J., Mather, T.A., Lacey, J.H., Wagner, B., Robinson, S.A., Pyle, D.M., Francke, A., Them II, T.R., and Panagiotopoulos, K.: Mercury records covering the past 90 000 years from lakes Prespa and Ohrid, SE Europe. *Biogeosciences* 21, 531–556. <https://doi.org/10.5194/bg-21-531-2024>, 2024.
- Pérez-Rodríguez, M., Biester, H., Aboal, J.R., Toro, M., and Martínez Cortizas, A.: Thawing of snow and ice caused extraordinary high and fast mercury fluxes to lake sediments in Antarctica. *Geochimica et Cosmochimica Acta* 248, 109–122. <https://doi.org/10.1016/j.gca.2019.01.009>, 2019.
- Pyle, D.M.: Widely dispersed Quaternary tephra in Africa. *Global and Planetary Change* 21, 95–112. [https://doi.org/10.1016/S0921-8181\(99\)00009-0](https://doi.org/10.1016/S0921-8181(99)00009-0), 1999.
- Pyle, D.M., Mather, T.A.: The importance of volcanic emissions for the global atmospheric mercury cycle. *Atmospheric Environment* 37, 5115–5124. <https://doi.org/10.1016/j.atmosenv.2003.07.011>, 2003.
- Ribeiro Guevara, S., Meili, M., Rizzo, A., Daga, R., and Arribère, M.: Sediment records of highly variable mercury inputs to mountain lakes in patagonia during the past millennium. *Atmospheric Chemistry and Physics* 10, 3443–3453. <https://doi.org/10.5194/acp-10-3443-2010>, 2010.
- Rytuba, J.J.: Mercury from mineral deposits and potential environmental impact. *Environmental Geology* 43, 326–338. <https://doi.org/10.1007/s00254-002-0629-5>, 2003.
- Schlüter, K.: Review: Evaporation of mercury from soils. An integration and synthesis of current knowledge. *Environmental Geology* 39, 249–271. <https://doi.org/10.1007/s002540050005>, 2000.
- Scholz, C.A., Johnson, T.C., Cohen, A.S., King, J.W., Peck, J.A., Overpeck, J.T., Talbot, M.R., Brown, E.T., Kalinsek, L., Amoako, P.Y.O., Lyons, R.P., Shanahan, T.M., Castañeda, I.S., Heil, C.W., Forman, S.L., McHargue, L.R., Beuning, K.R., Gomez, J., and Pierson, J.: East African megadroughts between 135 and 75 thousand years ago and bearing on early-modern human origins. *Proceedings of the National Academy of Sciences of the United States of America* 104, 16416–16421. <https://doi.org/10.1073/pnas.0703874104>, 2007.
- Schütze, M., Tserendorj, G., Pérez-Rodríguez, M., Rösch, M., and Biester, H.: Prediction of Holocene mercury accumulation trends by combining palynological and geochemical records of lake sediments (Black Forest, Germany). *Geosciences (Switzerland)* 8. <https://doi.org/10.3390/geosciences8100358>, 2018.
- Sebag, D., Garcin, Y., Adatte, T., Deschamps, P., Ménot, G., and Verrecchia, E.P.: Correction for the siderite effect on Rock-Eval parameters: Application to the sediments of Lake Barombi (southwest Cameroon). *Organic Geochemistry* 123, 126–135. <https://doi.org/10.1016/j.orggeochem.2018.05.010>, 2018.
- Selin, N.E.: Global biogeochemical cycling of mercury: a review. *Annual Review of Environmental Resources* 34, 43–63, 2009.
- Shanahan, T.M., Beck, J.W., Overpeck, J.T., McKay, N.P., Pigati, J.S., Peck, J.A., Scholz, C.A., Heil, C.W., and King, J.: Late Quaternary sedimentological and climate changes at Lake Bosumtwi Ghana: New constraints from laminae analysis and radiocarbon age modeling. *Palaeogeography, Palaeoclimatology, Palaeoecology* 361–362, 49–60. <https://doi.org/10.1016/j.palaeo.2012.08.001>, 2012.
- Shanahan, T.M., Overpeck, J.T., Wheeler, C.W., Beck, J.W., Pigati, J.S., Talbot, M.R., Scholz, C.A., Peck, J., and King, J.W.: Paleoclimatic variations in West Africa from a record of late Pleistocene and Holocene lake level stands of Lake Bosumtwi, Ghana. *Palaeogeography, Palaeoclimatology, Palaeoecology* 242, 287–302. <https://doi.org/10.1016/j.palaeo.2006.06.007>, 2006.
- Shanahan, T.M., Peck, J.A., McKay, N., Heil, C.W., King, J., Forman, S.L., Hoffmann, D.L., Richards, D.A., Overpeck, J.T., and Scholz, C.: Age models for long lacustrine sediment records using multiple dating

- approaches - An example from Lake Bosumtwi, Ghana. *Quaternary Geochronology* 15, 47–60.
<https://doi.org/10.1016/j.quageo.2012.12.001>, 2013.
- Skonieczny, C., McGee, D., Winckler, G., Bory, A., Bradtmiller, L.I., Kinsley, C.W., Polissar, P.J., De Pol-Holz, R., Rossignol, L., and Malaizé, B.: Monsoon-driven Saharan dust variability over the past 240,000 years. *Science Advances* 5, 1–9. <https://doi.org/10.1126/sciadv.aav1887>, 2019.
- Sun, Y., McManus, J.F., Clemens, S.C., Zhang, X., Vogel, H., Hodell, D.A., Guo, F., Wang, T., Liu, X., and An, Z.: Persistent orbital influence on millennial climate variability through the Pleistocene. *Nature Geoscience* 14, 812–818. <https://doi.org/10.1038/s41561-021-00794-1>, 2021.
- Tjallingii, R., Claussen, M., Stuut, J.-B.W., Fohlmeister, J., Jahn, A., Bickert, T., Lamy, F., and Röhl, U.: Coherent high- and low-latitude control of the northwest African hydrological balance. *Nature Geosci* 1, 670–675. <https://doi.org/10.1038/ngeo289>, 2008.
- Ulfers, A., Zeeden, C., Voigt, S., Sardar Abadi, M., and Wonik, T.: Half-precession signals in Lake Ohrid (Balkan) and their spatio-temporal relations to climate records from the European realm. *Quaternary Science Reviews* 280, 107413. <https://doi.org/10.1016/j.quascirev.2022.107413>, 2022.
- United Nations Environment Programme.: *Global Mercury Assessment*, United Nations, 2018.
- Vidal, C.M., Fontijn, K., Lane, C.S., Asrat, A., Barfod, D., Tomlinson, E.L., Piermattei, A., Hutchison, W., Tadesse, A.Z., Yirgu, G., Deino, A., Moussallam, Y., Mohr, P., Williams, F., Mather, T.A., Pyle, D.M., and Oppenheimer, C.: Geochronology and glass geochemistry of major Pleistocene eruptions in the Main Ethiopian Rift: Towards a regional tephrostratigraphy. *Quaternary Science Reviews* 290, 107601. <https://doi.org/10.1016/j.quascirev.2022.107601>, 2022.
- Vindušková, O., Jandová, K., and Frouz, J.: Improved method for removing siderite by *in situ* acidification before elemental and isotope analysis of soil organic carbon. *J. Plant Nutr. Soil Sci.* 182, 82–91. <https://doi.org/10.1002/jpln.201800164>, 2019.
- Wang, X., Bao, Z., Lin, C.-J., Yuan, W., and Feng, X.: Assessment of Global Mercury Deposition through Litterfall. *Environ. Sci. Technol.* 50, 8548–8557. <https://doi.org/10.1021/acs.est.5b06351>, 2016.
- Wang, X., Piao, S., Ciais, P., Friedlingstein, P., Myneni, R.B., Cox, P., Heimann, M., Miller, J., Peng, S., Wang, T., Yang, H., and Chen, A.: A two-fold increase of carbon cycle sensitivity to tropical temperature variations. *Nature* 506, 212–215. <https://doi.org/10.1038/nature12915>, 2014.
- Weldeab, S., Lea, D.W., Schneider, R.R., and Andersen, N.: 155,000 Years of West African Monsoon and Ocean Thermal Evolution. *Science* 316, 1303–1307. <https://doi.org/10.1126/science.1140461>, 2007.
- Whitlock, C., and Larsen, C.: Charcoal as a Fire Proxy, in: Smol, J.P., Birks, H.J.B., Last, W.M., Bradley, R.S., Alverson, K. (Eds.), *Tracking Environmental Change Using Lake Sediments, Developments in Paleoenvironmental Research*. Springer Netherlands, Dordrecht, pp. 75–97. https://doi.org/10.1007/0-306-47668-1_5, 2022.
- Yost, C.L., Jackson, L.J., Stone, J.R., and Cohen, A.S.: Subdecadal phytolith and charcoal records from Lake Malawi, East Africa imply minimal effects on human evolution from the ~ 74 ka Toba supereruption. *Journal of Human Evolution* 116, 75–94. <https://doi.org/10.1016/j.jhevol.2017.11.005>, 2018.
- Zhou, J., Obrist, D., Dastoor, A., Jiskra, M., and Ryjkov, A.: Vegetation uptake of mercury and impacts on global cycling. *Nature Reviews Earth and Environment* 2, 269–284. <https://doi.org/10.1038/s43017-021-00146-y>, 2021.
- Zhou, J., Wang, Z., and Zhang, X.: Deposition and Fate of Mercury in Litterfall, Litter, and Soil in Coniferous and Broad-Leaved Forests. *Journal of Geophysical Research: Biogeosciences* 123, 2590–2603. <https://doi.org/10.1029/2018JG004415>, 2018.